Recovery Kinetics in Commercial Purity Aluminum Deformed to Ultrahigh Strain: Model and Experiment

Yu, Tianbo; Hansen, Niels

Published in:
Metallurgical and Materials Transactions A: Physical Metallurgy and Materials Science

Link to article, DOI:
10.1007/s11661-016-3581-9

Publication date:
2016

Document Version
Peer reviewed version

Recovery Kinetics in Commercial Purity Aluminum Deformed to Ultrahigh Strain – Model and Experiment

Tianbo YU* and Niels HANSEN

Section for Materials Science and Advanced Characterization, Department of Wind Energy, Risø Campus, Technical University of Denmark, DK-4000, Roskilde, Denmark

*tiyu@dtu.dk

Abstract:

A new approach to analyze recovery kinetics is developed from a recent model, and microstructural observations are introduced to supplement hardness measurements. The approach involves two steps of data fitting, and the second step of fitting enables an estimation of the apparent activation energy for recovery. This approach is applied to commercial purity aluminum (AA1050) cold rolled to ultrahigh strain (99.6% reduction in thickness) and annealed at temperatures from 413 K (140 °C) to 493 K (220 °C). The annealing data fit the recovery model well and the analysis shows that the apparent activation energy increases during recovery and approaches 190 kJ/mol at the end of recovery, suggesting that solute drag is an important rate-controlling mechanism. The recovery rate for the highly strained Al is found to be higher than that for Al deformed to a lower strain, an effect which is related to an increase in the stored energy or driving force. These findings form the basis for a discussion of recovery mechanisms and the increase in the apparent activation energy during annealing, suggesting an application of the model when optimizing the structure and strength through annealing of nanostructured materials produced by high strain deformation.

I. INTRODUCTION

In the last two decades, great effort has been put into producing nanostructured materials by plastic deformation to large strains.[1,2] Strong ultrafine-grained or nanostructured materials can now be produced by a number of routes, but their thermal stability and formability are critical for industrial application. After deformation to a large strain, the structure typically has a high stored energy and a lamellar morphology composed of finely spaced extended lamellar boundaries and interconnecting boundaries in-between, although the aspect ratio is affected by the deformation mode.[3–5] During recovery annealing, the dislocation density decreases and the structure coarsens, reducing the strength and enhancing the formability.[6–8] Thus there is a possibility to optimize the properties of nanostructured materials by recovery annealing. However, the annealing conditions must be defined accurately to avoid extensive loss in strength due to occurrence of recrystallization, i.e. the recovery kinetics is of both scientific and technological importance.

Studies of recovery processes and kinetics encompass parameters such as annealing time and temperature, the applied strain, and the purity of the material.[9–15] In the literature recovery processes have been studied in detail in aluminum deformed to medium to high strains; it has been confirmed that such processes occur simultaneously or concurrently and that they can proceed towards nucleation of recrystallization.[7,12,16–19] A follow-up is therefore to study kinetics in an attempt to identify the individual processes in play. This is the objective of the present study, and an important parameter is therefore the activation energy, which relates to the rate controlling mechanism of recovery and also bridges the recovery kinetics among different annealing temperatures.

In the current study, a new approach to analyze recovery kinetics is presented and applied as an example to heavily deformed Al based on hardness measurements. This approach is based on a recovery model suggested by Vandermeer and Hansen.[20] The Al has a purity of 99.5% and was cold rolled to a thickness reduction of 99.6%, and therefore it has a typical deformation structure of a metal of medium/high stacking fault energy (e.g. Ni, Cu and Fe), having a finely spaced lamellar structure, a high stored energy and a high fraction of high angle boundaries – an ultrafine structure or a nanostructure.

II. RECOVERY KINETICS MODEL

Following Kuhlmann[9], Borelius and co-workers[21] suggested the following rate equation for recovery

$$\frac{dP}{dt} = -K_0 P \exp(-\frac{Q_0 - \beta P}{RT}), \qquad [1]$$

where P is the stored energy decreasing during annealing, t is the annealing time, R is the universal gas constant, T is the absolute temperature, Q_0 is the activation energy at the end of recovery, and the three fitting parameters K_0, Q_0 and β are associated with the operative recovery mechanisms. Eq. [1] may be recognized as a first-order reaction rate equation with an apparent activation energy depending linearly on the extent of recovery already occurred.

Based on Eq. [1], a model for recovery kinetics was suggested by Vandermeer and Hansen.[20] In that model, recovery is discussed in terms of f^2, which is defined as

$$f^2 = \left(\frac{H - H_r}{H_d - H_r} \right)^2, \qquad [2]$$

where H_d is the hardness of the deformed sample, H_r is the hardness of the completely recrystallized sample, and H is the hardness after recovery annealing. The parameter f^2 is assumed to be proportional to the stored energy or the driving force, thereby representing the deformed sample after partial annealing. In Eq. [1], when P is taken to be proportional to f^2 and with the aid of exponential integrals, the following equation can be obtained (f^2=1 when t=0)

$$E_1\{\frac{\beta P_0 f^2}{RT}\} = E_1\{\frac{\beta P_0}{RT}\} + tt_0^{-1}, \qquad [3]$$

where E_1 is the exponential integral of the quantity inside the bracket, P_0 is the deformation stored energy before annealing, and t_0^{-1} is a temperature dependent constant, which can be expressed as

$$t_0^{-1} = K_0 \exp(-\frac{Q_0}{RT}). \qquad [4]$$

The apparent activation energy Q_{app} and the internal state variable f^2 are related as

$$Q_{app} = Q_0 - \beta P_0 f^2. \qquad [5]$$

The hardness H (and thereby f^2) may include contributions from both recovered regions and recrystallized grains when recrystallization initiates. Therefore in the model by Vandermeer and Hansen, the hardness of the recovered region was calculated by removing the effect of the recrystallized grains based on an assumption of recrystallization kinetics.[20] In the current study, however, we incorporate microstructural characterization in order to determine the onset of recrystallization and exclude partially recrystallized samples in the analysis.

To estimate the model parameters t_0^{-1} and $\beta P_0/R$ at each annealing temperature, the values of (t, f^2) pairs are inserted into Eq. [3] and a curve of t_0^{-1} vs $\beta P_0/R$ is calculated for each (t, f^2) pair. Then at each temperature, a maximum convergence point

($\beta P_0/R$, t_0^{-1}) is determined manually by superimposing t_0^{-1} vs $\beta P_0/R$ curves of all annealing times where only recovery has taken place. The model thus gives a fitting of the recovery kinetics. By extrapolating to longer annealing times, the contribution of discontinuous recrystallization may be factored out from samples where recovery and recrystallization take place simultaneously.

It should be pointed out that in the above fitting, the values of t_0^{-1} and $\beta P_0/R$ are assumed to be temperature dependent, and thus they may give information on different recovery mechanisms operating at different temperatures. However, in order to estimate the apparent activation energy, one has to assume the same mechanisms operating at different annealing temperatures, i.e. the fitting parameters K_0, Q_0 and β (and thus also $\beta P_0/R$) have to be the same at all temperatures. Therefore a second fitting step, only for t_0^{-1}, may be carried out by taking the average value of $\beta P_0/R$ from the first fitting step. Such a procedure enables accurate estimation of the apparent activation energy, and significantly improves the model applicability.[20,22]

III. EXPERIMENTAL DETAILS

AA1050 aluminum, with an initial grain size of ~100 μm and a main chemical composition of 99.5Al-0.25Fe-0.15Si (wt %), was cold rolled to a true strain of 5.5 (99.6% reduction in thickness). The material is similar to those in our previous studies.[17,18] Immediately after rolling, one piece of the deformed material was stored in a freezer, whereas others were kept at room temperature. After storage for about 400 days, a number of smaller samples were cut from the material kept at room temperature, and subjected to an isothermal heat treatment at temperatures of 413, 433, 453, 473 and 493 K (140, 160, 180, 200 and 220 °C) over time intervals ranging from 1 minute to 51

days. The heat treatments for less than 1 hour were carried out in an oil bath, whereas longer treatments were conducted in air furnaces. After annealing, the samples were cold mounted in epoxy resin and mechanical polished on the longitudinal section containing the rolling direction (RD) and the normal direction (ND), and Vickers hardness tests were carried out on the polished surface with a load of 50 g and a holding time of 10 s. The hardness value at each condition was taken as the average of at least eight measurements. The hardness of the deformed state and of the fully recrystallized state, annealed at 773 K (500 °C) for 4 h, was also measured.

The microstructures of the annealed samples were determined in the longitudinal section (ND-RD section) by electron backscatter diffraction (EBSD) mapping in a field emission gun-scanning electron microscope (FEG-SEM). Samples for EBSD analysis were mechanically polished followed by electropolishing at 277 K (4 °C) for 45 s in a solution of ethanol (70 pct), water (12 pct), 2-butoxy-ethanol (10 pct), and perchloric acid (8 pct) using a voltage of 13 V. Step sizes of 0.1~3 μm were used in order to identify the initiation of recrystallization. In the current study, both hardness tests and EBSD investigations were carried out at the sample thickness center, where typical high strain structure and texture prevail.[17]

IV. EXPERIMENT AND MODEL

The Vickers hardness numbers of the deformed Al were 51.2±0.8 and 47.3±0.7 for samples stored in the freezer and kept at room temperature, respectively. The decrease in hardness indicates that recovery has taken place at room temperature during long-term exposure, which has been analyzed in a previous study, where hardness was measured on the rolling plane with a load of 200 g.[19] A simple extrapolation from the

previous result shows that this part of recovery finishes in one minute when annealed at 473 K (200 °C). Therefore the hardness of the deformed state was taken as $H_d = 51.2$ in the kinetics analysis in order to include an initial stage of recovery. It was also found that the general conclusion was unchanged if $H_d = 47.3$ was taken in the kinetics analysis, and therefore only results based on $H_d = 51.2$ will be reported in the following.

The hardness variation during isothermal annealing is shown in Figure 1. These curves indicate that a slight hardening may be superimposed on recovery during the early stages of annealing. The hardening may be due to dislocation source limited hardening[23] or precipitation hardening as precipitates can be observed at longer annealing times.[19] However, an analysis of this initial hardening is beyond the scope of the present work, and samples annealed at 413 K (140 °C) and 433 K (160 °C) for less than one hour were not included in the kinetics analysis.

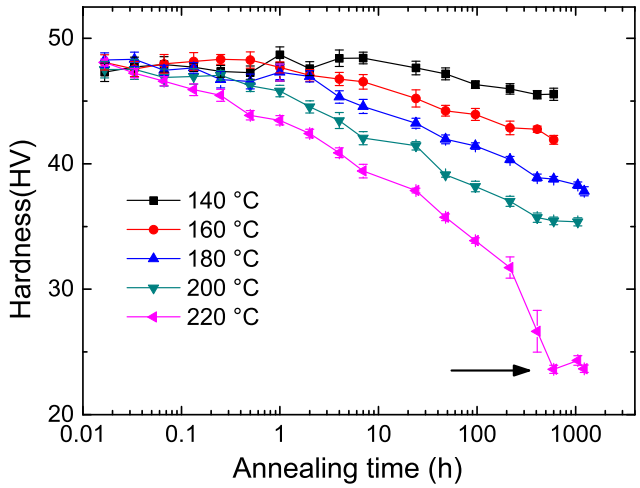

Fig. 1—Hardness variation of heavily cold-rolled Al during isothermal annealing. Error bars show the standard deviations.

EBSD analysis of selected samples showed that there was no discontinuous recrystallization in samples annealed at 473 K (200 °C) or below. Characteristic nuclei

started to form after annealing at 493 K (220 °C) for 96 h (Figure 2), in agreement with the hardness curves, where large standard deviations at longer annealing times suggests a composite structure of recovered and recrystallized regions. Therefore samples annealed at 493 K (220 °C) for 96 h and longer were not included in the kinetics analysis. The hardness of the fully recrystallized state (H_r) was measured to be 24.6±0.4, also in agreement with the hardness of samples annealed at 493 K (220 °C) for the three longest times as shown in Figure 1 and marked with an arrow.

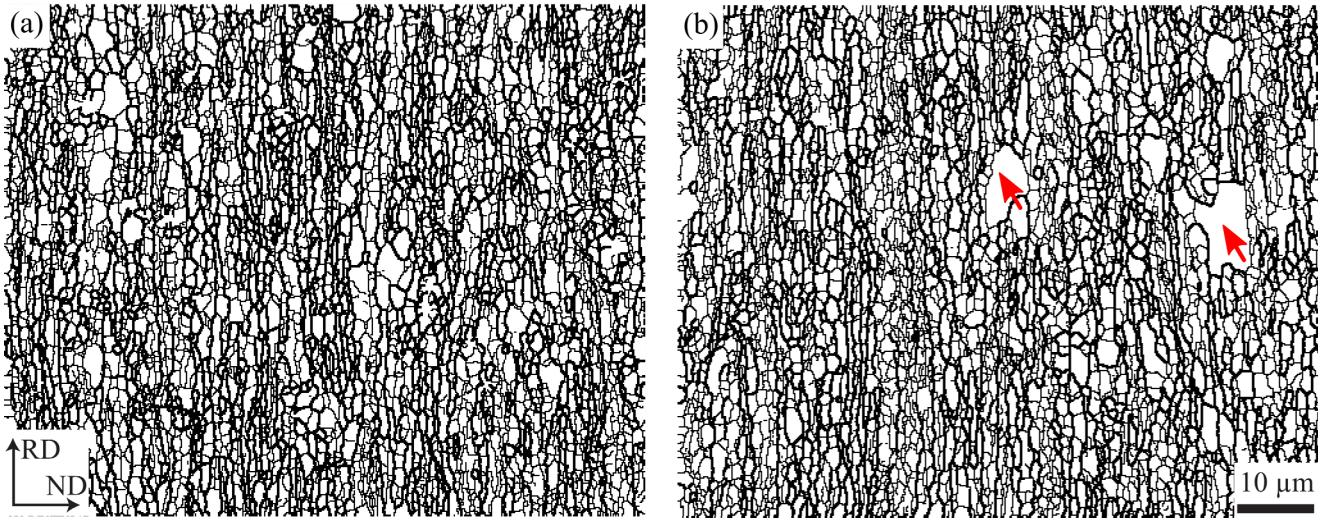

Fig. 2—Boundary structures revealed by EBSD in the longitudinal plane of the Al sample after annealing at (a) 473 K (200 °C) for 600 h and (b) 493 K (220 °C) for 96 h. High angle boundaries (>15°) are shown in bold lines and low angle boundaries (1.5~15°) in thin lines. The coarsening at 473 K (200 °C) was relatively uniform, whereas discontinuous recrystallization initiated (see red arrows) after 96 h annealing at 493 K (220 °C)

Based on the above measurements, the experimental recovery parameters (i.e. the convergence points) determined for individual temperatures are listed in Table I. The parameter $\beta P_0/R$ decreases with increasing temperature, and therefore according to

Eq. [5] it can be deduced that at a given recovery stage (i.e. fixing f^2) the apparent activation energy Q_{app} increases with increasing temperature when Q_0 is assumed to be constant. This finding indicates that several recovery processes with different activation energies are operative during annealing. Based on the parameters shown in Table I, the corresponding recovery kinetics curves at different temperatures are drawn in Figure 3.

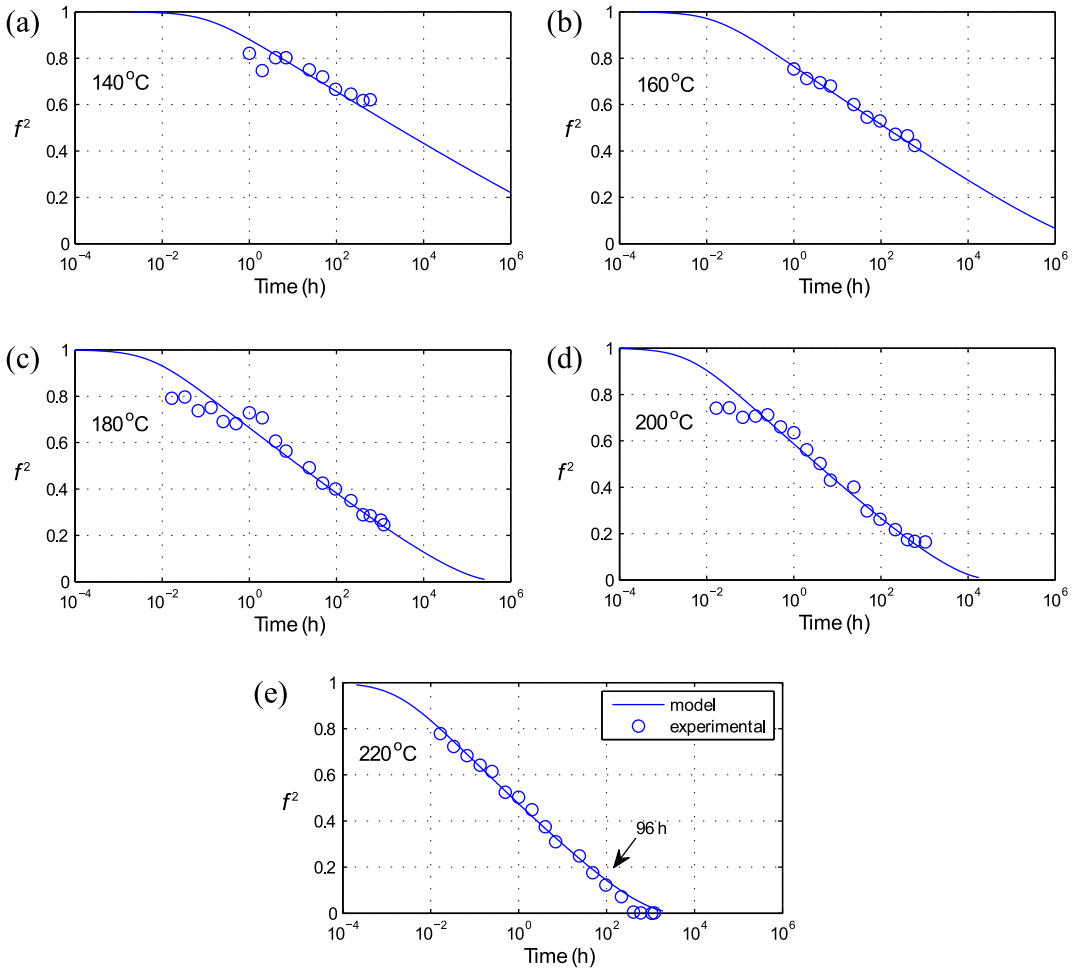

Fig. 3—Isothermal kinetics of recovery of heavily cold-rolled Al. The curves are fitted independently at five different temperatures. See Eq. [2] for the definition of f^2.

Table I. Experimental Recovery Parameters Determined Independently at Different Temperatures for Heavily Cold-rolled Al.

Temperature (K)	t_0^{-1} (h^{-1})	$\beta P_0/R$ (K)
413 (140 °C)	3.1×10^{-9}	7.8×10^{3}
433 (160 °C)	1.8×10^{-7}	7.3×10^{3}
453(180 °C)	5.9×10^{-6}	6.6×10^{3}
473 (200 °C)	9.2×10^{-5}	5.8×10^{3}
493 (220 °C)	9.1×10^{-4}	5.4×10^{3}

The curves in Figure 3 are fitted independently. However, in order to estimate the apparent activation energy, one has to fit the recovery curves collectively, i.e. using the same fitting parameters K_0 and $\beta P_0/R$ for all temperatures. It can be calculated from Table I that the average value of $\beta P_0/R$ is 6.6×10^3 K. When this average value is used for all temperatures, one obtains the collective fitting of the recovery kinetics as shown in Figure 4. The fitting curves in Figure 4 are slighly different from those in Figure 3. The collective fitting, where K_0 is a constant indpendent of temperature, allows us to estimate Q_0 according to Eq. [4]. Based on the fittings in Figure 4, the corresponding values of t_0^{-1} are ploted against $1000/T$ in Figure 5, leading to $K_0 = 1.2\times10^{16}$ h^{-1} and the activation energy at the end of recovery (f^2=0) Q_0 = 186±10 kJ/mol. According to Eq. [5], the apparent activation energy at the beginning of recovery (f^2=1) can then be calculated as 131 kJ/mol.

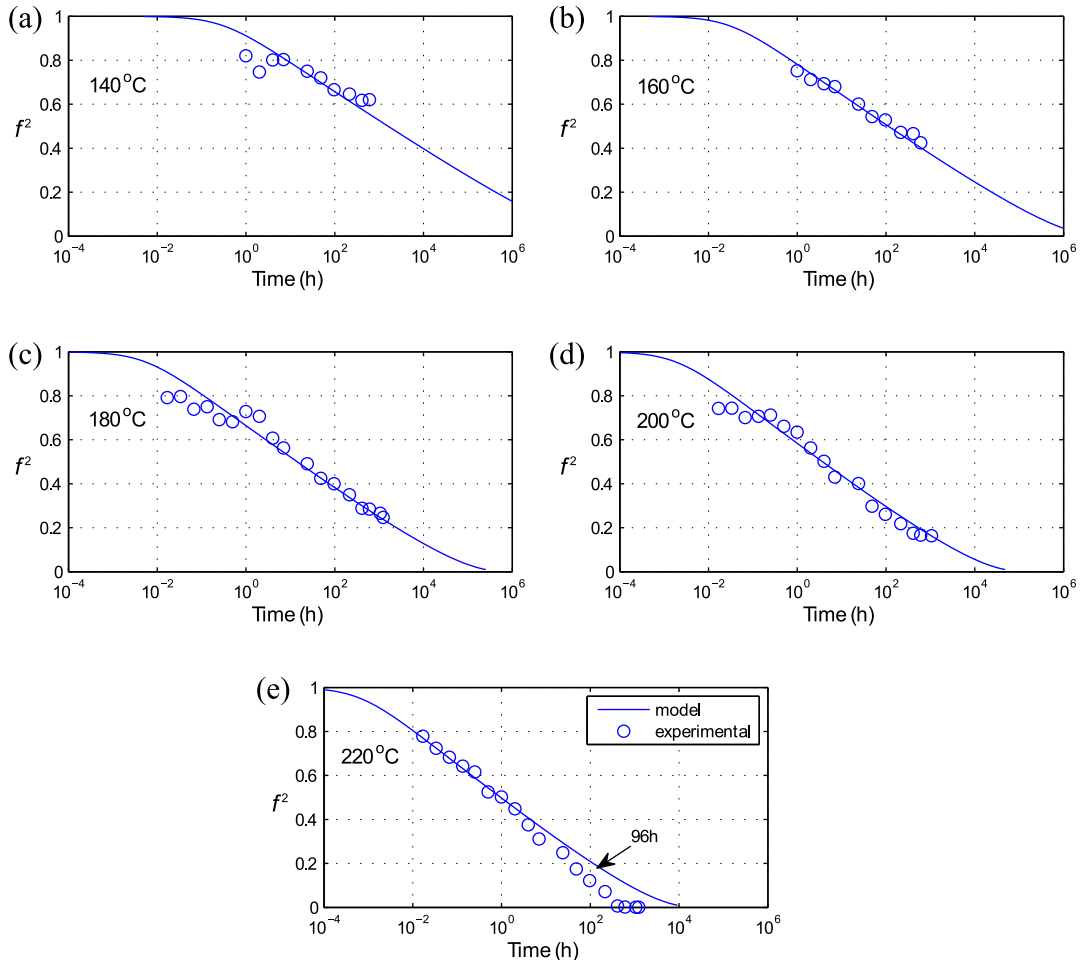

Fig. 4—Isothermal kinetics of recovery of heavily cold-rolled Al. The curves are fitted collectively using the same fitting parameters (K_0, Q_0 and β) at five different temperatures.

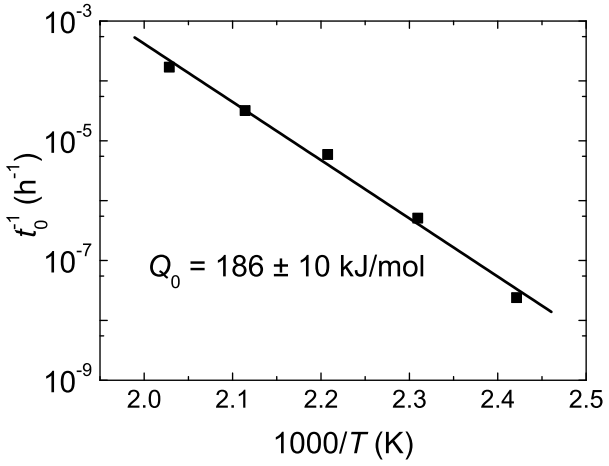

Fig. 5—Temperature dependence of recovery kinetics in heavily cold-rolled Al.

V. Validation of the kinetics model

Eq. [1] allows the apparent activation energy to change in the course of recovery (see Eq. [5]), and the obtained positive values of the fitting parameter $\beta P_0/R$ (see Table I) suggest that the apparent activation energy increases during recovery, in agreement with previous studies.[9,10,14,18,20] Moreover, Eq. [1] assumes a linear change of the apparent activation energy against f^2 during recovery, and the good fittings shown in Figures 3 and 4 indicate that such an assumption is reasonable.

The parameter f^2 was favored by Vandermeer and Hansen[20] due to its relatability to the dislocation density and the stored energy, and is thus adopted in the current model to follow recovery kinetics. However, the fraction f is also often used to measure the state of recovery.[10,14] If f^2 is replaced by f, similar analyses can be carried out. In this case, more weight is given to samples annealed at longer times and slightly higher activation energies are estimated (Q_0 = 215±5 kJ/mol compared to Q_0 = 186±10 kJ/mol). However, the general conclusion is unchanged, and a good agreement between two analyses therefore appears.

A direct validation of the kinetics model is based on a comparison of experimental observations and model predictions. As examples, Figure 6 shows the predicted recovery kinetics at 543 K (270 °C) and 573 K (300 °C), which are about 60 and 500 times faster than that at 493 K (220 °C), respectively. The predicted kinetics at 573 K (300 °C) indicates a significant recovery after annealing for 1 minute (f^2 decreases to 0.39), in a good agreement with microstructural observations from another study of AA1050 aluminum deformed to a true strain of 5.5.[17]

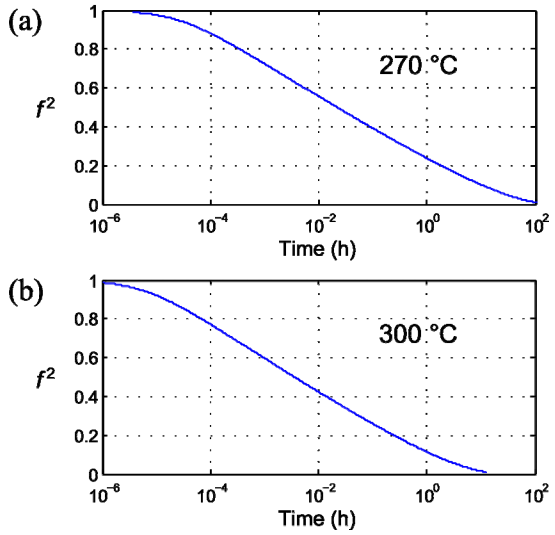

Fig. 6—Predicted recovery kinetics of heavily cold-rolled AA1050 aluminum at (a) 543 K (270 °C) and (b) 573 K (300 °C).

VI. DISCUSSION

The deformation microstructure after a high strain contains dislocations and deformation-induced high and low angle boundaries of different energy, and different recovery processes for example dislocation annihilation and reconfiguration,[24] subgrain growth,[11] and triple junction motion[15] may operate concurrently or consecutively. As pointed out by Bever, different processes may have different kinetics, and therefore one relationship is only an approximation.[8] Furthermore, even for a single recovery process, the rate controlling mechanisms are also complex. For example in the present Al different impurity elements may have a significant effect, and therefore interpretation of the modelling results must be done with some caution.

A. *Activation Energy and Recovery Mechanisms*

The observed change of apparent activation energy for recovery processes may shed light on activated fundamental mechanisms. In an attempt to identify such

mechanisms the experimental data were analyzed by dividing the recovery into small windows and assuming a constant activation energy (Q) within each window, in analogy to the analysis of coarsening of lamellar structure reported recently.[18] Based on the following equation

$$\ln t = c + \frac{Q}{RT}, \qquad [6]$$

where c is a constant for a given recovery window, the activation energy for each recovery window can be calculated by comparing the annealing time intervals used at different temperatures to obtain the same degree of recovery (e.g. f^2 decreases from 0.5 to 0.4). Such an analysis led to a stepwise increase of the activation energy as shown in Figure 7, where the linear change calculated from the current model is also shown for comparison. Generally the two approaches agree, supporting the simplification on activation energy applied in the current model.

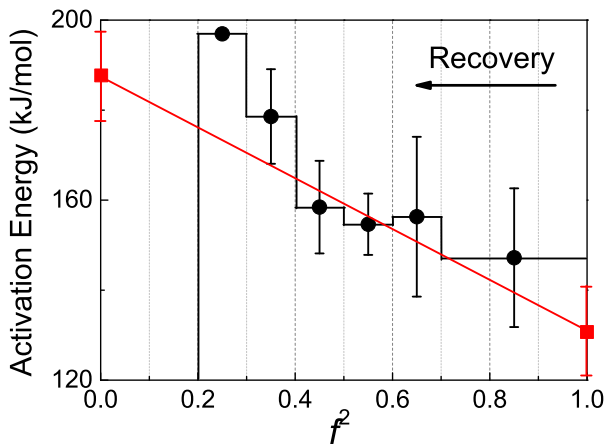

Fig. 7—Variation of the activation energy against f^2 during recovery of heavily cold-rolled Al. The linear curve is derived from the current model, and the stepwise curve is calculated based on Eq. [6]. The error bars are calculated based on the standard errors of linear least squares fittings.

Table II. Activation Energies for Different Diffusion Mechanisms in Al.

Mechanism	Diffusion species	Diffusion path	Activation energy (kJ/mol)
Vacancy diffusion	Vacancy	Lattice	62.6[25]
Self-diffusion	Al	Lattice	126[26]
Pipe diffusion	Al	Dislocation	82[36]
Boundary diffusion	Al	Boundary	53[37]
Diffusion of Fe	Fe	Lattice	183-259[38,39]
Diffusion of Si	Si	Lattice	129-154[40]

Recovery mechanisms may be closely related to diffusion mechanisms.[6] The activation energies for several diffusion mechanisms in Al are listed in Table II. Those for vacancy diffusion and self-diffusion have been studied extensively and well documented,[25,26] but this is not the case for diffusion along boundaries and dislocation cores, and the often-cited activation energy for boundary diffusion, 84 kJ/mol, was derived from a rough estimation.[27] Table II also lists the activation energies for diffusion of two solute atoms Fe and Si through Al lattice. During annealing of a heavily deformed metal, the microstructure coarsens, inevitably involving migration of high and low angle boundaries. The activation energy for boundary migration depends strongly on the purity of the material.[28] In high purity Al the activation energy was found to be low (73 kJ/mol) for this process.[29] However in Al alloys, solutes segregate at boundaries, causing solute drag during boundary migration.[30,31] Therefore lattice diffusion of solutes is usually considered as a rate controlling mechanism during subgrain growth, recrystallization and grain growth.[14,20,32–34] An apparent activation energy for recovery may not directly correspond to an ideal diffusion mechanism since the deformation structure is complex. Nevertheless, in the present study Q_0 = 186

kJ/mol, as well as Q_0 = 215 kJ/mol if f is used instead of f^2, is consistent with the diffusion of iron in the bulk of Al as was also found in the end of subgrain growth[14] and during recrystallization[35] of similar Al.

A low activation energy typically indicates that a process is easy to operate. Excess vacancies produced by plastic deformation can be annealed out below room temperature in Al with a very low activation energy, 60 kJ/mol as reported by Schmidt and Haessner.[13] Further annealing results in recovery of mobile dislocations with a slightly higher activation energy,[19] whereas significant grain/subgrain coarsening occurs at later stages with an activation energy increasing from 110 to 240 kJ/mol as reported recently.[18] In the present study, the decrease of hardness is mainly due to grain/subgrain coarsening, and the result is consistent with the coarsening kinetics reported previously.[18] A number of factors may contribute to the increases of the activation energy. During grain/subgrain coarsening the total boundary area decreases, and therefore the concentration of solutes in the boundaries may increase, leading to an increasingly pronounced effect of solute drag.[41] The grain/subgrain coarsening before recrystallization is dominated by triple junction motion, and such a coarsening pattern may be associated with a lower activation energy than that for normal boundary migration – due to the special geometry solutes may be deposited at the tailing boundary of a migrating triple junction and exert a relatively weak drag effect. As the boundary spacing increases and the morphology changes, an increase in the activation energy for triple junction motion is expected. Moreover, with increasing boundary spacing and decreasing dislocation density during recovery, the contribution from boundary diffusion and pipe diffusion decreases, leading to a higher apparent activation energy.

B. The Strain Effect

The recovery and recrystallization behavior in AA1050 aluminum deformed to a strain of 5.5 was previously found to be different between the thickness center and the subsurface region,[17] and the current study has focused on the thickness center. The recovery kinetics in the subsurface region of Al cold-rolled to strains 2, 4 and 5.5 has been analyzed tentatively based on hardness measurements on the rolling plane with a load of 200 g, and it was found that the recovery rate increases with increasing strain.[20,22] In the following, the previous data of strains 4 and 5.5 from the subsurface region are analyzed based on the new approach – collective fitting. Fixing the value of $\beta P_0/R$ for each strain (see Table III) and fitting the recovery curves collectively, one gets the corresponding values of t_0^{-1} at different temperatures as plotted in Figure 8. For both strains, good linear fittings can be obtained over the whole temperature range (this was not possible using the previous approach[20,22]), and the corresponding values for K_0 and Q_0 are listed in Table III. The larger values of $\beta P_0/R$ and t_0^{-1} for Al deformed to a higher strain reveal the strain effect on recovery – a lower initial activation energy and a higher recovery rate. As shown in Table III, the estimated activation energies at the end of recovery are in good agreement with the present analysis of recovery in the thickness center of Al deformed to a strain of 5.5 (see Figure 5). This agreement suggests that despite different recovery rates due to difference in local stored energy and microstructure, the fundamental recovery mechanisms are similar.

Table III. Experimental Recovery Parameters Determined through Collective Fitting for the Subsurface Region of Cold-rolled Al.

Strain	$\beta P_0/R$ (K)	K_0 (h^{-1})	Q_0 (kJ/mol)
4	5.3×10^3	1.5×10^{16}	192±5
5.5	6.8×10^3	1.4×10^{17}	196±11

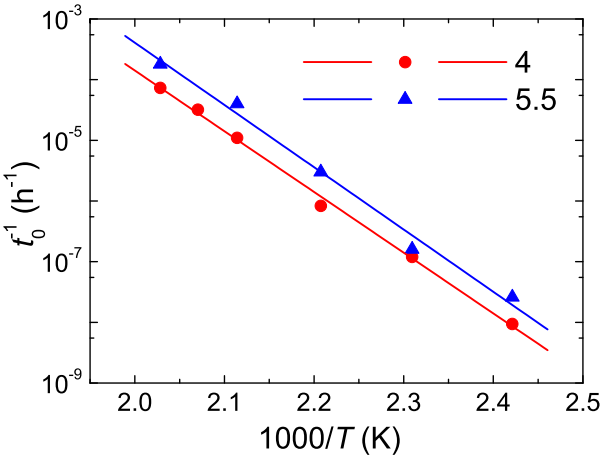

Fig. 8—Temperature dependence of recovery kinetics in the subsurface region of cold-rolled Al at two different strains.

VII. CONCLUSION

1. A new approach to analyze recovery kinetics is developed from a recent model, and microstructural observations are introduced to supplement hardness measurements. This approach involves two steps of data fitting, where the second step enables an estimation of the apparent activation energy.

2. The new approach has been applied to commercial purity aluminum (AA1050) cold-rolled to an ultrahigh strain ($\varepsilon_t = 5.5$) and annealed in the temperature range 413-493 K (140-220 °C). It has been found that the apparent activation energy

increases by about 55 kJ/mol in the course of recovery reaching about 190 kJ/mol at the end of recovery.

3. The change in the apparent activation energy with recovery stage is related to fundamental recovery mechanisms. No direct correlations have been identified except that at later stages solute drag appears as an important rate controlling mechanism in the aluminum of commercial purity.

4. In general the suggested approach to analyze recovery kinetics may be a useful tool in the endeavor to produce strong and ductile materials by thermomechanical processing. This is of special importance in the development of ultrafine-grained or nanocrystalline materials applying plastic deformation to ultrahigh strains, where the enhancement in strength is counterbalanced by a loss in ductility, and where solutions are still in demand.

ACKNOWLEDGEMENTS

The authors gratefully acknowledge the support from the Danish National Research Foundation (Grant No. DNRF86-5) and the National Natural Science Foundation of China (Grant No. 51261130091) to the Danish-Chinese Center for Nanometals, within which part of this work has been performed.

REFERENCES

1. N. Hansen: *Metall. Mater. Trans. A*, 2001, vol. 32, pp. 2917–2935.

2. Y. Estrin and A. Vinogradov: *Acta Mater.*, 2013, vol. 61, pp. 782–817.

3. D. A. Hughes and N. Hansen: *Acta Mater.*, 2000, vol. 48, pp. 2985–3004.

4. R. Z. Valiev and T. G. Langdon: *Prog. Mater. Sci.*, 2006, vol. 51, pp. 881–981.

5. H. W. Zhang, X. Huang, and N. Hansen: *Acta Mater.*, 2008, vol. 56, pp. 5451–5465.

6. F. J. Humphreys and M. Hatherly: *Recrystallization and Related Annealing Phenomena*, 2nd ed., Pergamon Press, Oxford, 2004.

7. E. Nes: *Acta Metall. Mater.*, 1995, vol. 43, pp. 2189–2207.

8. M. B. Bever: *Creep and Recover,*American Society for Metals, Cleveland, OH, 1957, pp. 14-51.

9. D. Kuhlmann: *Zeitschrift Fur Phys.*, 1948, vol. 124, pp. 468–481.

10. J. T. Michalak and H. W. Paxton: *TMS-AIME*, 1961, vol. 221, pp. 850–857.

11. C. J. E. Smith and I. L. Dillamore: *Met. Sci.*, 1970, vol. 4, pp. 161–167.

12. R. Sandstrom: *Acta Metall.*, 1977, vol. 25, pp. 905–911.

13. J. Schmidt and F. Haessner: *Zeitschrift Fur Phys. B*, 1990, vol. 81, pp. 215–222.

14. T. Furu, R. Ørsund, and E. Nes: *Acta Metall. Mater.*, 1995, vol. 43, pp. 2209–2232.

15. T. Yu, N. Hansen, and X. Huang: *Proc. R. Soc. A*, 2011, vol. 467, pp. 3039–3065.

16. A. R. Jones, B. Ralph, and N. Hansen: *Proc. R. Soc. A*, 1979, vol. 368, pp. 345–357.

17. O. V Mishin, A. Godfrey, D. J. Jensen, and N. Hansen: *Acta Mater.*, 2013, vol. 61, pp. 5354–5364.

18. T. Yu, N. Hansen, and X. Huang: *Acta Mater.*, 2013, vol. 61, pp. 6577–6586.

19. T. Yu, N. Hansen, and X. Huang: *Philos. Mag.*, 2012, vol. 92, pp. 4056–4074.

20. R. A. Vandermeer and N. Hansen: *Acta Mater.*, 2008, vol. 56, pp. 5719–5727.

21. G. Borelius, S. Berglund, and S. Sjoberg: *Ark. Fys.*, 1952, vol. 6, pp. 143–149.

22. T. Yu, N. Hansen, X. Huang, and G. Winther: *Proc. 30th Risø Int. Symp. Mater. Sci.*, Risø DTU, Roskilde, Denmark, 2009, pp. 393–400.

23. X. Huang, N. Hansen, and N. Tsuji: *Science*, 2006, vol. 312, pp. 249–251.

24. R. Sandstrom: *Acta Metall.*, 1977, vol. 25, pp. 897–904.

25. W. Desobro and D. Turnbull: *Phys. Rev.*, 1959, vol. 115, pp. 560–563.

26. T. E. Volin and R. W. Balluffi: *Phys. Status Solidi*, 1968, vol. 25, pp. 163–173.

27. H. J. Frost and M. F. Ashby: *Deformation Mechanism Maps*, Pergamon press, New York, 1982.

28. G. Gottstein and L. S. Shvindlerman: *Grain Boundary Migration in Metals*, 2nd ed., CRC Press, Boca Raton, FL, 2010.

29. F. Haessner and J. Schmidt: *Acta Metall. Mater.*, 1993, vol. 41, pp. 1739–1749.

30. K. Lucke and K. Detert: *Acta Metall.*, 1957, vol. 5, pp. 628–637.

31. J. W. Cahn: *Acta Metall.*, 1962, vol. 10, pp. 789–798.

32. Y. Huang and F. J. Humphreys: *Acta Mater.*, 1999, vol. 47, pp. 2259–2268.

33. Y. Huang and F. J. Humphreys: *Acta Mater.*, 2000, vol. 48, pp. 2017–2030.

34. H. Jazaeri, F. J. Humphreys, and P. S. Bate: *Mater. Sci. Forum*, 2006, vol. 519-521, pp. 153–160.

35. R. A. Vandermeer and D. Juul Jensen: *Acta Mater.*, 2001, vol. 49, pp. 2083–2094.

36. T. E. Volin, K. H. Lie, and R. W. Balluffi: *Acta Metall.*, 1971, vol. 19, pp. 263–274.

37. L. L. Levenson: *Appl. Phys. Lett.*, 1989, vol. 55, pp. 2617–2619.

38. D. L. Beke, I. Godney, I. A. Szabo, G. Erdelyi, and F. J. Kedves: *Philos. Mag. A*, 1987, vol. 55, pp. 425–443.

39. G. M. Hood: *Philos. Mag.*, 1970, vol. 21, pp. 305–328.

40. L. F. Mondolfo: *Aluminum Alloys: Structure and Properties*, Butterworths, London, 1976.

41. D. A. Molodov, U. Czubayko, G. Gottstein, and L. S. Shvindlerman: *Acta Mater.*, 1998, vol. 46, pp. 553–564.